Population extinction under bursty reproduction in a time-modulated environment

Ohad Vilk and Michael Assaf[*]

Racah Institute of Physics, Hebrew University of Jerusalem, Jerusalem 91904, Israel

In recent years nondemographic variability has been shown to greatly affect dynamics of stochastic populations. For example, nondemographic noise in the form of a bursty reproduction process with an *a priori* unknown burst size, or environmental variability in the form of time-varying reaction rates, have been separately found to dramatically impact the extinction risk of isolated populations. In this work we investigate the extinction risk of an isolated population under the *combined* influence of these two types of nondemographic variation. Using the so-called *momentum-space* Wentzel–Kramers–Brillouin (WKB) approach and accounting for the explicit time dependence in the reaction rates, we arrive at a set of time-dependent Hamilton equations. To this end, we evaluate the population's extinction risk by finding the instanton of the time-perturbed Hamiltonian numerically, whereas analytical expressions are presented in particular limits using various perturbation techniques. We focus on two classes of time-varying environments: periodically varying rates corresponding to seasonal effects and a sudden decrease in the birth rate corresponding to a catastrophe. All our theoretical results are tested against numerical Monte Carlo simulations with time-dependent rates and also against a numerical solution of the corresponding time-dependent Hamilton equations.

I. INTRODUCTION

Stochastic processes that result in the extinction of a stochastic population after maintaining a long-lived state, affect a wide range of biological populations, and have attracted much interest over the past decades. Manifestations of such stochastic processes range from population biology, epidemiology, cell biochemistry, virology, gene regulation, and conservational ecology, see, e.g., Refs. [1–8].

If the population is isolated, then there is always an absorbing state at zero. That is, extinction can occur due to a rare sequence of death events owing to *demographic noise*, which stems from the stochastic nature of the reactions and discreteness of individuals. While most previous studies of population extinction have focused on this type of noise, see e.g., Refs. [9–21], nondemographic variability (see, e.g., Refs. [22,23]) may dramatically influence the extinction risk of a population subject to demographic noise [24–36]. In general, nondemographic noise originates from the variability across individuals as well as from environmental variations and can give rise to time-varying reaction rates. These variations, however, are not necessarily stochastic and may be caused by deterministic factors such as seasonal shifts in temperature or humidity, competition, breeding sites, or forage availability, see, e.g., Refs. [37–39]. Notably, while these factors result in time-periodic reaction rates [16,25,31,35], a population can also experience, e.g., a sudden drastic drop in the birth rate due to a drastic deterioration of environmental conditions [17].

In addition to varying the reaction rates, nondemographic noise can also influence the reaction *step size*. Here, for example, instead of having a single birth event with a fixed number of products $A \rightarrow 2A$, nondemographic noise can give rise to a *bursty* reproduction process $A \rightarrow A + kA$, where $k = 0,1,2\ldots$ is a random non-negative integer that is drawn from a given step-size distribution. This type of uncertainty, or noise, appears in a wide variety of scientific areas including population biology and ecology [40], viral dynamics [8], and cell biology [41,42]. Importantly, such reaction step-size noise contributes to the variability in the ecological traits of a population and can strongly affect the extinction probability of a population [32,36,38].

In previous works, the extinction risk of a population has been studied separately under the influence of deterministically time-varying rates [16,17,31,35] and reaction step-size noise [32,33,36]. In reality, however, both these effects ought to be taken into account. For example, seasonal variations of temperature can cause a time modulation in the reaction rates, while fluctuations in the offspring number per birth event (which also depends on the seasonal variability) cause an uncertainty in the reaction step size. As a result, in this paper we study how the extinction risk of a population is influenced under the combined effect of time-varying reaction rates and uncertainty in the reaction step size, thus generalizing previous works in this field [16,17,31,35]. For concreteness our starting point is the generalized version of the Verhulst logistic model with bursty reproduction that has been studied in Refs. [32,36]. To this end, using the momentum-space Wentzel–Kramers–Brillouin (WKB), or eikonal approach [11,13,14,19], we generalize the derivation done in Refs. [32,36] to allow dealing with explicitly time-dependent Hamiltonians and calculate the mean time to extinction (MTE) for generic step-size distributions (SSDs).
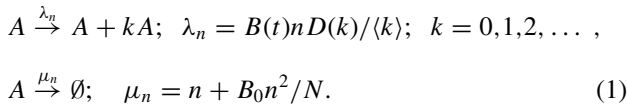
The paper is organized as follows. In Sec. II, we employ the generating function formalism in order to transform the master equation into a partial differential equation for the probability

_____

[*]michael.assaf@mail.huji.ac.il

generating function. Then we apply the eikonal method to this equation, which yields in the leading order a Hamilton-Jacobi equation with an effective (explicitly) time-dependent Hamiltonian. The latter also accounts for the uncertainty in the reaction step size due to the bursty reproduction. To this end, we analyze the corresponding Hamiltonian flow in various limits. In Sec. III we follow Assaf *et al.* [16] and apply three perturbation techniques, in three different regimes, to a population with time-periodic rates. The first regime is when the modulation amplitude is small, and a linear theory (LT) with respect to the modulation amplitude can be applied (Sec. III A). In the second regime, in the limit of high modulation frequency, we employ a formalism in the spirit of the Kapitsa method [43] (Sec. III B), while in the third low-modulation frequency regime, we employ an adiabatic theory (Sec. III C). Furthermore, in Sec. IV we consider a different time dependence of the reaction rates in the form of a finite and predetermined drop in the birth rate and compute the corresponding increase in the extinction risk of the population [17]. We dedicate Sec. V to a short description of the time-dependent Monte Carlo simulation that we have used as well as to describe how we solve the explicitly time-dependent Hamilton equations using the shooting method. Finally, in Sec. VI, we discuss the interplay between the two forms of nondemographic variability that we have considered.

II. MASTER EQUATION, PROBABILITY GENERATING FUNCTION, AND THE UNPERTURBED ACTION

Our starting point is the generalized Verhulst model with bursty reproduction [33]. The microscopic dynamics of our system are given by the following birth-death reactions with the corresponding rates:

$$A \xrightarrow{\lambda_n} A + kA; \quad \lambda_n = B(t)nD(k)/\langle k \rangle; \quad k = 0,1,2,\dots,$$

$$A \xrightarrow{\mu_n} \emptyset; \quad \mu_n = n + B_0 n^2/N. \tag{1}$$

Here n is the population size and $N \gg 1$ is the typical population size in the long-lived metastable state prior to extinction, see below. Also, the burst size k is *a priori* unknown and is drawn from a normalized SSD, $D(k)$, with a mean value of $\langle k \rangle$ and standard deviation σ. In addition, the birth rate per capita satisfies $B(t) = B_0 g(t)$, where $g(t)$ is a known function of time and $B_0 > 1$ is the average reproduction rate per capita.

Using Eq. (1), the deterministic (mean-field) dynamics is governed by the following rate equation: $\dot{\bar{n}} = \bar{n}[B(t) - 1 - B_0 \bar{n}/N]$. In the time-independent case, $B(t) = B_0$, this equation has a stable fixed point at $\bar{n} = N(B_0 - 1)/B_0$, and an unstable fixed point at $\bar{n} = 0$. Henceforth, we will assume $N \gg 1$; that is, the typical population size at the stable fixed point is large. In Fig. 1 we present the typical mean-field dynamics of $\bar{n}(t)$ for a periodic birth rate.

The rate equation ignores demographic fluctuations. To account for these, and to compute the MTE, we consider the master equation describing the time evolution of the probability $\mathcal{P}_n(t)$ of having n individuals at time t. Using Eq. (1) the master
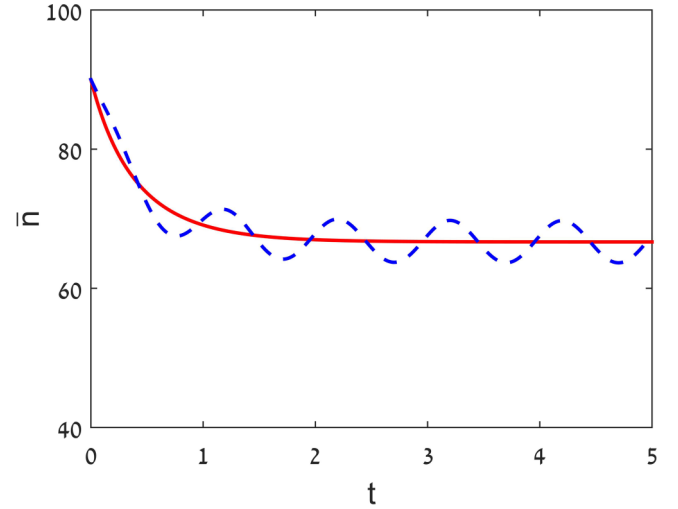

FIG. 1. Numerical solution of the rate equation, see text: a comparison between the time-perturbed (dashed line) and unperturbed (solid) cases. Parameters are $B_0 = 3$ and $N = 200$ for both cases, while the birth rate in the perturbed case is given by $B(t) = B_0[1 + \epsilon \cos(\omega t)]$ with $\epsilon = 0.1$ and $\omega = 1$.

equation reads

$$\dot{\mathcal{P}}_n = \frac{B(t)}{\langle k \rangle}\left[\sum_{k=0}^{n-1} D(k)(n-k)\mathcal{P}_{n-k} - n\mathcal{P}_n\right]$$
$$+ (n+1)\mathcal{P}_{n+1} - n\mathcal{P}_n + \frac{B_0}{N}[(n+1)^2\mathcal{P}_{n+1} - n^2\mathcal{P}_n]. \tag{2}$$

Note that the rate equation described above can be obtained from this master equation by multiplying the latter by n, summing over all n's, and using the definition $\bar{n}(t) = \sum_n n\mathcal{P}_n(t)$.

To treat master equation (2) we introduce the probability generating function [3] $G(\wp,t) = \sum_{n=0}^{\infty} \wp^n \mathcal{P}_n(t)$, with $\wp$ being an auxiliary variable. Note that $\mathcal{P}_n(t)$ is given by the Taylor coefficients of $G(\wp,t)$ around $\wp = 0$. Multiplying Eq. (2) by $\wp^n$ and summing over all n's, we arrive at a partial differential equation for $G(\wp,t)$,

$$\frac{\partial G}{\partial t} = (\wp - 1)\left\{\left[B(t)\wp f(\wp) - 1 - \frac{B_0}{N}\right]\frac{\partial G}{\partial \wp} - \frac{B_0}{N}\wp\frac{\partial^2 G}{\partial \wp^2}\right\}, \tag{3}$$

where we have defined $f(\wp) = \sum_{k=0}^{\infty} D(k)(\wp^k - 1)/[\langle k \rangle(\wp - 1)]$, which is related to the probability generating function of the SSD. Assuming $N \gg 1$, employing the eikonal ansatz $G(\wp,t) \sim \exp[-NS(\wp,t)]$ in Eq. (3), where $S(\wp)$ is the action function [11], and neglecting subleading-order terms with respect to N, we arrive at a Hamilton-Jacobi equation

$$\frac{\partial S}{\partial t} = (\wp - 1)\left\{[B(t)\wp f(\wp) - 1]\frac{\partial S}{\partial \wp} + B_0\wp\left(\frac{\partial S}{\partial \wp}\right)^2\right\}. \tag{4}$$

Introducing a canonically conjugate coordinate $q = -\partial S/\partial \wp$, and shifting the momentum $p = \wp - 1$ [44], we arrive at the following one-dimensional Hamiltonian flow,

where p plays the role of the momentum [11]:

$$H(t) = pq[B(t)(p+1)f(p+1) - 1 - B_0(p+1)q], \quad (5)$$

and to remind the reader, $B(t) = B_0 g(t)$. At this point we note that in the time-*independent* case, Eq. (5) coincides, up to a canonical transformation, with the Hamiltonian obtained in Ref. [33]. The corresponding Hamilton equations are

$$\dot{q} = q[B(t)(2p+1)f(p+1) - 1 - B_0(2p+1)q \\ + B(t)p(p+1)f'(p+1)], \quad (6)$$

$$\dot{p} = -p[B(t)(p+1)f(p+1) - 1 - B_0(p+1)2q]. \quad (7)$$

For completeness we begin by outlining the results obtained in Ref. [33] for the time-*independent* case, and then we generalize the results to the time-dependent case. When the rates are constant, Hamiltonian (5) is conserved and the problem is integrable. The most probable path to extinction, often referred to as the optimal path to extinction or instanton [9], is a nontrivial zero-energy trajectory of (5) and is given by

$$q_0(p_0) = f(p_0 + 1) - \frac{1}{B_0(p_0 + 1)}. \quad (8)$$

The corresponding action along the instanton satisfies

$$S_0 = -\int_0^{p_f} q_0(p)dp = \frac{1}{B_0}\ln(1 + p_f) - \int_0^{p_f} f(p+1)dp, \quad (9)$$

where p_f is the momentum associated with the fluctuational fixed point, $(q = 0, p = p_f)$, which can be found by solving the transcendental equation $f(p_f + 1) = 1/[B_0(p_f + 1)]$. In the leading order, the MTE is given by $\tau \sim \exp(N S_0)$ [11]. Note that having found p_f, the action S_0 can be evaluated by substituting the exact form of $f(p+1)$ into Eq. (9) [33].

III. PERIODIC ENVIRONMENT

Let us now assume that the time modulation is periodic, $g(t) = 1 + \epsilon \cos(\omega t)$. The time-dependent Hamiltonian (5) is now given by

$$H(q,p,t) = H_0(q,p) + \epsilon H_1(q,p,t), \quad (10)$$

where

$$H_0(q,p) = pq[B_0(p+1)f(p+1) - 1 - B_0(p+1)q] \quad (11)$$

and

$$H_1(q,p,t) = pqB_0(p+1)f(p+1)\cos(\omega t). \quad (12)$$

To compute the MTE up to leading order we need to find the action along the perturbed instanton of the time-dependent Hamiltonian. Denoting the coordinates of the perturbed path by $q(t,t_0)$ and $p(t,t_0)$, a general expression for the action can be written as [16]

$$S = \int_{-\infty}^{\infty} \{p(t,t_0)\dot{q}(t,t_0) - H_0[q(t,t_0), p(t,t_0)] \\ - \epsilon H_1[q(t,t_0), p(t,t_0), t]\}dt, \quad (13)$$

where t_0 is the phase element of the Poincaré map which gives the minimal action [45–47]. As mentioned above, this problem can be analytically solved only in specific limits. Following Ref. [16] we now apply three perturbation techniques in three different parameter regimes.

A. Linear theory

In this subsection we assume that the time perturbation is small, i.e., $\epsilon \ll 1$. Let us define by $q_0(t - t_0)$ and $p_0(t - t_0)$ the coordinate and momentum of the unperturbed zero-energy instanton evaluated at time $t - t_0$ [48]. For $\epsilon \ll 1$, it has been shown that the action can be approximated as [16,45–47]:

$$S(t_0) \simeq S_0 + \Delta S(t_0), \quad (14)$$

where S_0 is the unperturbed action (9) and

$$\Delta S(t_0) = -\epsilon \int_{-\infty}^{\infty} H_1[q_0(t - t_0), p_0(t - t_0), t]dt. \quad (15)$$

To find the optimal correction, $\Delta S(t_0)$ must be *minimized* with respect to t_0. Substituting Eq. (8) into Eq. (7), we arrive at the following integral equation:

$$t(p_0) = t_0 + \int^{p_0} \frac{dp_0}{p_0[B_0(p_0 + 1)f(p_0 + 1) - 1]}, \quad (16)$$

where the integration constant was absorbed in t_0. Further, using Eqs. (7) and (8) one finds along the unperturbed instanton $\dot{p} = B_0 qp(p+1)$. Employing the latter and Eq. (12), Eq. (15) becomes

$$\Delta S(t_0) = -\epsilon \int_0^{p_f} f(p_0 + 1)\cos(\omega t)dp_0, \quad (17)$$

where p_f is the fluctuational momentum defined above and t is a function of p_0 as indicated by Eq. (16). Note that a particular choice of the SSD, $D(k)$, determines the form of $f(p)$ in both Eq. (16) and (17). Finally, to find the minimal action, solution (17) has to be minimized with respect to t_0. As a result, and as was previously shown by Dykman *et al.* [9,45,46], we find that in the LT the modulation signal removes the degeneracy of the unperturbed instanton trajectories with respect to the arbitrary time shift t_0. It is thus possible to select the optimal instanton in relation to the modulation signal.

Having found t_0 for which the correction to the action is minimal, the MTE is given by

$$\tau \sim e^{N(S_0 + \Delta S)}. \quad (18)$$

where $\Delta S = \min_{t_0}[\Delta S(t_0)]$ is negative and $\Delta S(t_0)$ is given by Eq. (17). This indicates that the time modulation brings about an exponential *increase* in the population's extinction risk, by a factor of $e^{N|\Delta S|}$.

Before considering particular examples, let us discuss the validity of the LT. The conditions for the general linear correction to hold is that $\epsilon \ll 1$ and

$$S_0 + \Delta S \gg 1/N. \quad (19)$$

Strictly speaking, we also need to separately demand that $|\Delta S| \gg 1/N$ for the eikonal approximation to hold [16], but our numerical results indicate that the theory works well already when $N|\Delta S| \gtrsim \mathcal{O}(1)$, see below. In Fig. 2 we compare the theoretical MTE [Eq. (18)] with numerical Monte
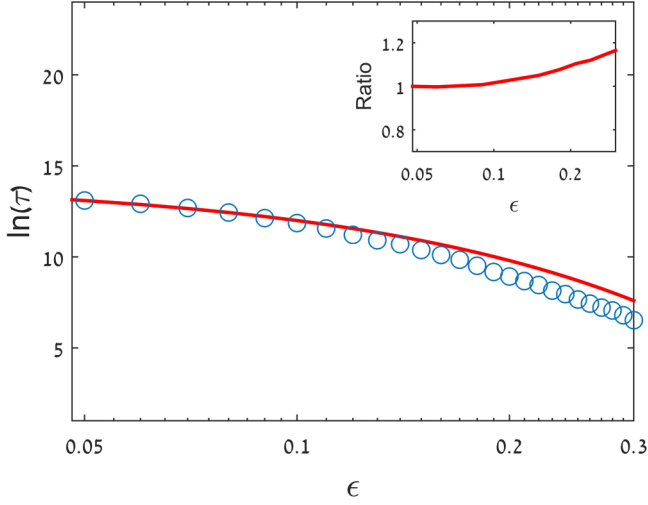
FIG. 2. The logarithm of the MTE in the LT regime for the case of binomial SSD as a function of ϵ: a comparison between the theoretical result (solid line) and Monte Carlo simulations with time-dependent rates (symbols). The parameters are $B_0 = 1.2$, $N = 3200$, $\omega = 0.24$, $m = 15$, and $\rho = 0.4$. Here the theoretical MTE (that does not include a preexponential prefactor) is multiplied by a constant so that it coincides with the numerical result at $\epsilon = 0.05$. Inset shows the ratio between the theoretical and numerical results. Note that the range of ϵ is such that $N|\Delta S| \gtrsim \mathcal{O}(1)$, see text.

FIG. 3. A comparison between the theoretical (solid line) and numerical (symbols) actions in the case of the SSR, in the LT regime, as a function of ϵ. The numerical solution is obtained by numerically calculating the instanton trajectory of the perturbed Hamiltonian. The parameters are $B_0 = 4$ and $\omega = 3$. Inset shows a numerical calculation of t_0 which minimizes the action, as a function of ϵ, see Sec. V. Here t_0 is measured in units of π/ω, and one can see that as long as $\epsilon \ll 1$, the theoretical prediction of $t_0 = \pi/\omega$ holds well.

Carlo simulations in the case of a binomial SSD. A detailed description of the Monte Carlo simulation with time-dependent rates that we have used, is found in Sec. V. The parameters for the binomial SSD are the number of trials m and the probability of success in each trial ρ. The figure demonstrates that the LT holds well as long as $\epsilon \ll 1$.

In the next two subsections we will find the explicit reduction of the action in two simple cases: the case of single-step reaction (SSR), $D(k) = \delta_{k,1}$, and for a general SSD close to the bifurcation limit.

1. Linear theory—SSR

In the SSR case, $D(k) = \delta_{k,1}$, we substitute $f(p) = 1$ into Eq. (16) and find $t(p_0)$, which can then be plugged into Eq. (17). After some algebra, $S(t_0)$ can be shown to satisfy the following integral:

$$\Delta S(t_0) = \epsilon \frac{B_0 - 1}{B_0} \int_{-\infty}^{\infty} \frac{1}{1 + e^{-x}} \frac{1}{1 + e^x}$$
$$\times \cos\left(\frac{\omega}{B_0 - 1} x + \omega t_0\right) dx, \quad (20)$$

which yields

$$\Delta S(t_0) = \frac{\epsilon \pi \omega}{B_0} \cos(\omega t_0) \operatorname{csch}\left(\frac{\pi \omega}{B_0 - 1}\right), \quad (21)$$

where $\operatorname{csch}(z) = 1/\sinh(z)$. Minimizing the action with respect to t_0 we find that $t_0 = \pi/\omega$, which yields the correction to the action for the SSR case [31],

$$\Delta S_{\text{SSR}} = -\frac{\epsilon \pi \omega}{B_0} \operatorname{csch}\left(\frac{\pi \omega}{B_0 - 1}\right). \quad (22)$$
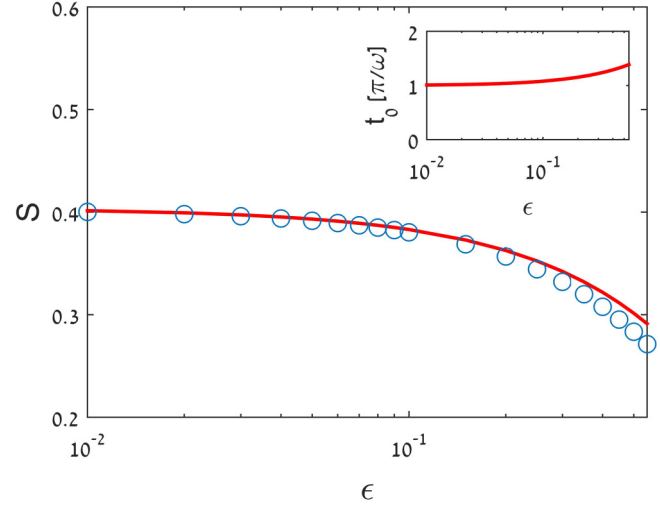
Before we continue it is informative to look at this result in two limits. In order to do so, we define by $\alpha \equiv \omega/(B_0 - 1)$ the ratio between the system's relaxation timescale $\sim (B_0 - 1)^{-1}$ and the timescale of the modulation $\sim \omega^{-1}$. In the adiabatic limit, $\alpha \ll 1$, where the modulation is slow, the correction to the action reduces to $\Delta S_{\text{SSR}} = -\epsilon(B_0 - 1)/B_0$, which coincides with our adiabatic approximation result for the SSR, presented in Sec. III C. On the other hand, in the high-frequency limit, $\alpha \gg 1$, where the modulation is rapid, the LT correction to the action becomes exponentially small in α, and the dominant term in ΔS becomes the $\mathcal{O}(\epsilon^2)$ term [16], see Sec. III B.

In Fig. 3 we compare the theoretical action with a numerical solution of the Hamilton equations (see Sec. V for a detailed description) in the SSR case. Excellent agreement is observed as long as $\epsilon \ll 1$. Here the theoretical action is given by $S = S_0 + \Delta S$, where ΔS is given by Eq. (22) while S_0 is given by Eq. (9) with $f(p) = 1$, which yields [18]

$$S_0 = 1 - \frac{1}{B_0} - \frac{1}{B_0} \ln(B_0). \quad (23)$$

Note that the numerical solution of the Hamilton equations also allows finding t_0 for which the action is minimal; to illustrate this point the inset of Fig. 3 shows t_0 as a function ϵ.

2. Linear theory—bifurcation limit

For general SSDs, an analytical solution for the action in the LT regime can only be found close to the bifurcation limit, where $0 < B_0 - 1 \ll 1$. To this end we *a priori* assume the momentum is small throughout the instanton trajectory (to be justified *a posteriori*). We denote $p_0 = (B_0 - 1)/[1 + f'(1)]\tilde{p}_0$,
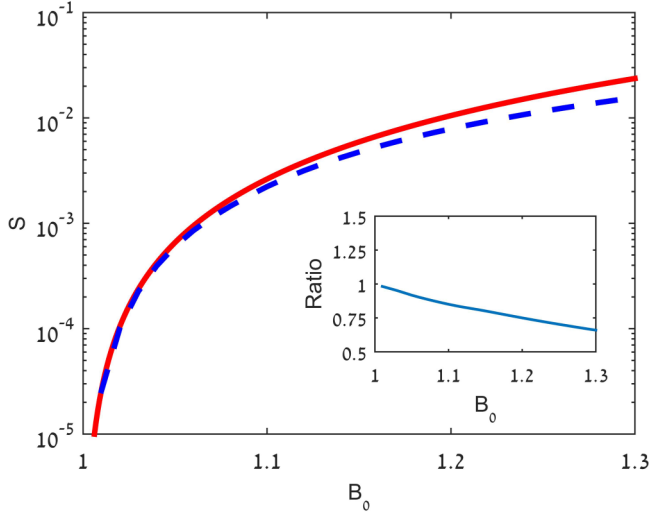
FIG. 4. A comparison between the LT theoretical action close to the bifurcation limit (solid line) and the general LT theoretical action (dashed line) for the case of a binomial SSD, as a function of B_0. The theoretical action at the bifurcation limit is given by Eqs. (25) and (26) while the general LT action is given by Eqs. (16), (17), and (9). The parameters are $\epsilon = 0.05$, $\omega = 1$, $m = 10$, and $\rho = 0.2$. Inset shows the ratio between the dashed and solid lines as a function of B_0.

where $\tilde{p}_0 = \mathcal{O}(1)$, and $f'(1)$ is found using L'Hôpital's rule,

$$f'(1) = \frac{1}{2}\left(\frac{\sigma^2}{\langle k \rangle} + \langle k \rangle - 1\right). \tag{24}$$

Substituting p_0 into Eqs. (16) and (17), keeping leading-order terms with respect to $B_0 - 1 \ll 1$, and minimizing the action with respect to t_0, we find that the minimum is obtained at $t_0 = \pi/\omega$. As a result, ΔS becomes

$$\Delta S \simeq -\epsilon \frac{\pi \omega}{1 + f'(1)} \operatorname{csch}\left(\frac{\pi \omega}{B_0 - 1}\right), \tag{25}$$

where the unpertubed action in this case satisfies [33]

$$S_0 = \frac{1}{2}\frac{(B_0 - 1)^2}{1 + f'(1)}. \tag{26}$$

Note that in the SSR case where $f'(1) = 0$, Eq. (25) reduces to Eq. (22) close to bifurcation. Also note that, using Hamilton equations (6) and (7), the unperturbed instanton trajectory satisfies $q(t - t_0) = (B_0 - 1)/[1 + e^{(B_0-1)(t-t_0)}]$ and $p(t - t_0) = -(B_0 - 1)/\{[1 + f'(1)][1 + e^{-(B_0-1)(t-t_0)}]\}$, thus justifying *a posteriori* our assumption regarding the smallness of the momentum. Finally, the result given by Eqs. (25) and (26) is valid as long as $S = S_0 + \Delta S \gg 1/N$, which puts an upper limit on the value of ϵ, depending on the value of $\alpha = \omega/(B_0 - 1)$.

In Fig. 4 we demonstrate that the theoretical result for the action close to bifurcation, given by Eqs. (25) and (26), converges to the general result obtained in Sec. III A as B_0 approaches the value of 1.

B. Kapitsa correction

In this subsection we consider the high-frequency limit, $\alpha \gg 1$, in which the modulation frequency is high compared to the typical relaxation rate of the system. The Kapitsa method was originally developed in the context of the "Kapitsa pendulum," see, e.g., Ref. [43], and here we apply a Hamiltonian extension of the method along the same lines of Ref. [16].

We begin with Hamiltonian (5) and denote

$$q(t) = Q(t) + \frac{B_0}{B_0 - 1}\xi(t),$$
$$p(t) = P(t) + \frac{B_0}{B_0 - 1}\eta(t), \tag{27}$$

where Q and P are slowly changing variables, and ξ and η are rapidly changing, small corrections. Expanding $H(q, p, t)$ [given by Eq. (5)] around $q = Q$ and $p = P$ up to second order in ξ and η yields

$$H(q, p, t)$$
$$\simeq H(Q, P, t) + \xi \frac{\partial H(Q, P, t)}{\partial Q} + \eta \frac{\partial H(Q, P, t)}{\partial P}$$
$$+ \xi^2 \frac{\partial^2 H(Q, P, t)}{\partial Q^2} + \eta^2 \frac{\partial^2 H(Q, P, t)}{\partial P^2} + \xi\eta \frac{\partial^2 H(Q, P, t)}{\partial P \partial Q}$$
$$\equiv \tilde{H}(Q, P, t). \tag{28}$$

Using Eqs. (27) and (28) the Hamilton equations become

$$\dot{q} = \dot{Q} + \frac{B_0}{B_0 - 1}\dot{\xi} \simeq \frac{\partial \tilde{H}(Q, P, t)}{\partial P},$$
$$\dot{p} = \dot{P} + \frac{B_0}{B_0 - 1}\dot{\eta} \simeq -\frac{\partial \tilde{H}(Q, P, t)}{\partial Q}. \tag{29}$$

Demanding that the rapidly oscillating terms balance each other, we obtain

$$\dot{\xi} = \epsilon(B_0 - 1)\cos(\omega t)Q[(2P + 1)f + P(P + 1)f']$$
$$\dot{\eta} = -\epsilon P(B_0 - 1)(P + 1)f\cos(\omega t), \tag{30}$$

where $f = f(P + 1)$. Treating Q and P as constants, we can solve these equations to find

$$\xi = \frac{\epsilon}{\alpha}\sin(\omega t)Q[(2P + 1)f + P(P + 1)f']$$
$$\eta = -\frac{\epsilon}{\alpha}\sin(\omega t)P(P + 1)f. \tag{31}$$

From this result it is clear that since $\alpha \gg 1$, $\epsilon \leqslant 1$ does not need to be small in order for this approximation scheme to be valid.

We now employ a canonical transformation to transform from the old (q, p) to the new (Q, P) variables, see Appendix A for details. The effective Hamiltonian, averaged over a period of a rapid oscillation $2\pi/\omega$, becomes

$$\bar{H}(Q, P) = H_0(Q, P) + \left(\frac{\epsilon}{\alpha}\right)^2 H_2(Q, P), \tag{32}$$

where $H_0(Q, P)$ is the unperturbed Hamiltonian, given by Eq. (11), and $H_2(Q, P)$ is given by Eq. (A4) in Appendix A. Since this effective Hamiltonian is time *independent*, it is straightforward to find the effective instanton. Using Eq. (32), and repeating the steps that led to Eqs. (8) and (9), the instanton reads

$$Q(P) = Q_0(P) + \left(\frac{\epsilon}{\alpha}\right)^2 Q_K(P), \tag{33}$$
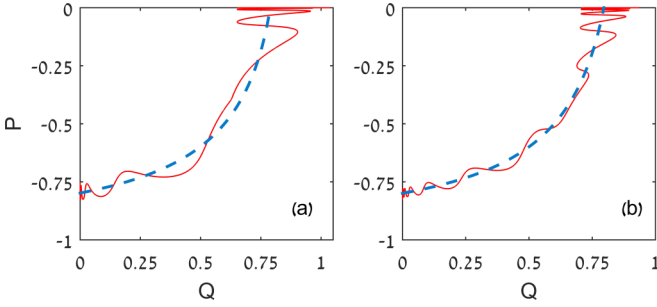
FIG. 5. Projections on the (Q, P) plane of instantons for two sets of parameters in the high-frequency regime. Here we compare the theoretical instanton (dashed line) given by Eqs. (33), (8), and (35), with the numerically found instanton (solid line), see Sec. V, for the SSR case. The parameters are $B_0 = 4$ and $\epsilon = 0.5$. In (a) $\alpha = 3$, and the theoretical correction to the action ΔS deviates by 30% from the numerical result. In (b) $\alpha = 5$, and the deviation of the theoretical result from the numerical one is 14%.

where $Q_0(P)$ is the unperturbed instanton (8), and $Q_K(P)$ is given by Eq. (A5) in Appendix A. As a result, the action becomes

$$S = -\int_0^{P_f} Q(P)dP = S_0 + \left(\frac{\epsilon}{\alpha}\right)^2 \Delta S_K, \qquad (34)$$

where the second term, $\Delta S_K \equiv \int_0^{P_f} Q_K(P)dP$, is the Kapitsa correction, while S_0 is given by Eq. (9).

Let us demonstrate this method by explicitly calculating the Kapitsa correction for the SSR case. Here $f(P) = 1$, and $Q_K(P)$ given by Eq. (A5) becomes

$$Q_K(P) = \frac{1 - B_0 + 3P - 4B_0 P - 4B_0 P^2}{2B_0}. \qquad (35)$$

Using the fact that in this case $P_f = -(B_0 - 1)/B_0$, the Kapitsa correction in Eq. (34) becomes [31]

$$\Delta S_K = \frac{1}{4B_0} - \frac{1}{6} - \frac{1}{12B_0^3}. \qquad (36)$$

Figure 5 shows examples of numerically found instantons, for two different values of α in the high-frequency regime. Here we compare for the SSR case the theoretical instanton trajectories given by Eq. (33) with Eqs. (8) and (35), with numerically found instantons, according to the recipe given in Sec. V. One can see that as α is increased, the numerical instanton and action along it, converge into the theoretical results.

1. Kapitsa correction—bifurcation limit

We now briefly present the results of the Kapitsa correction close to the bifurcation limit, $B_0 - 1 \ll 1$, by repeating the steps done in Sec. III A 2. Substituting $P = -(B_0 - 1)/[1 + f'(1)]\tilde{P}$ and $Q = \tilde{Q}(B_0 - 1)$ into $Q_K(P)$ [Eq. (A5) in Appendix A] and keeping only leading-order terms with respect to $B_0 - 1 \ll 1$, we arrive at

$$\tilde{Q}(\tilde{P}) \simeq \tfrac{1}{2}(\tilde{P} - 1). \qquad (37)$$

Using this result and the fact that $P_f = -(B_0 - 1)/[1 + f'(1)]$ in this limit, ΔS_K becomes

$$\Delta S_K = -\frac{1}{4}\frac{(B_0 - 1)^2}{1 + f'(1)}. \qquad (38)$$

Thus, the total action close to the bifurcation takes the following compact form:

$$S = S_0\left[1 - \frac{1}{2}\left(\frac{\epsilon}{\alpha}\right)^2\right], \qquad (39)$$

where S_0 is given by Eq. (26). Equation (39) is valid as long as $B_0 - 1 \ll \omega \ll (B_0 - 1)^{-1/2}$, namely, the frequency cannot be too high. This is because, on the one hand, the Kapitsa method requires $\alpha \gg 1$ or $\omega \gg B_0 - 1$, whereas on the other hand, in S we have neglected $\mathcal{O}(B_0 - 1)^3$ terms, while keeping terms of $\mathcal{O}[(B_0 - 1)^2\alpha^{-2}]$ (here $\epsilon \lesssim 1$).

C. Adiabatic approximation

In the adiabatic limit the modulation frequency is much smaller than the typical relaxation rate of the system, i.e., $\alpha \ll 1$. In this case we can consider an approximation that is nonperturbative in the modulation amplitude. It has been shown by Assaf *et al.* [16] that the average extinction rate $\bar{r}_{\text{ex}}$ in the adiabatic limit is

$$\bar{r}_{\text{ex}} = \frac{\omega}{2\pi}\int_0^{\frac{2\pi}{\omega}} r_{\text{ex}}(t')dt', \qquad (40)$$

with $r_{\text{ex}}(t)$ being the instantaneous value of the slowly time-dependant extinction rate. In this approximation the MTE is equal to $1/\bar{r}_{\text{ex}}$.

The mean extinction rate under bursty reproduction and constant reaction rates has been calculated by Be'er *et al.* [33], including pre-exponential corrections. Following the steps outlined in the Appendix of Ref. [33], the time-instantaneous extinction rate in our case is given by

$$r_{\text{ex}}(t) = A(t)e^{-NS[p_f(t),t]}, \qquad (41)$$

with

$$S(p,t) = \int_p^0 \left\{f(p'+1)[1 + \epsilon \cos(\omega t)] - \frac{1}{B_0(p'+1)}\right\}dp', \qquad (42)$$

and

$$A(t) = -p_f\{B_0[1 + \epsilon \cos(\omega t)] - 1\}\left[\frac{NS_{pp}(p_f,t)}{2\pi}\right]^{1/2}. \qquad (43)$$

Here p_f is explicitly time dependent and is defined by

$$f(p_f + 1)[1 + \epsilon \cos(\omega t)] = \frac{1}{B_0(p_f + 1)}, \qquad (44)$$

while $S_{pp}(p_f, t)$ is the second derivative of the action in Eq. (42) with respect to p evaluated at $p = p_f(t)$. Substituting Eq. (41) into Eq. (40), the average extinction rate is given by

$$\bar{r}_{\text{ex}} = \frac{\omega}{2\pi}\int_0^{\frac{2\pi}{\omega}} A(t')e^{-NS[p_f(t'),t']}dt'. \qquad (45)$$

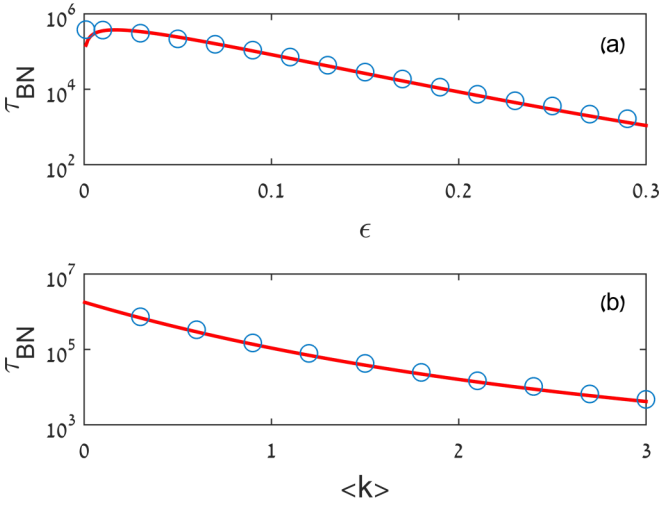FIG. 6. The MTE, τ_{BN}, for the case of a binomial SSD in the adiabatic regime: theory (solid line) versus Monte Carlo simulations (symbols). In (a) the MTE is plotted against ϵ, and the parameters are $B_0 = 3$, $\omega = 0.06$, $m = 10$, and $\rho = 0.3$. In (b) the MTE is plotted against the SSD's mean, $\langle k \rangle = m\rho$, and the parameters are $B_0 = 3$, $\omega = 0.06$, and $\epsilon = 0.3$.

which can be found via the saddle-point approximation

$$\bar{r}_{\mathrm{ex}} \simeq \frac{\omega}{2\pi} A(t_s) e^{-NS[p_f(t_s),t_s]} \left[\frac{2\pi}{N|S_{tt}[p_f(t_s),t_s]|} \right]^{1/2}. \quad (46)$$

Here the saddle point is found at $t_s = \pi/\omega$, and $S_{tt}[p_f(t_s),t_s]$ is the second derivative of action (42) with respect to t evaluated at t_s, while the time-dependent fluctuational momentum p_f has to also be evaluated at t_s according to Eq. (44). After some algebra, it can be shown that the average extinction rate becomes

$$\bar{r}_{\mathrm{ex}} \simeq C e^{-NS[p_f(t_s),t_s]}, \quad (47)$$

where S is given by Eq. (42). Here the pre-exponent

$$C = -p_f[B_0(1-\epsilon)-1] \left[\frac{(1-\epsilon)f'(p_f+1) + \frac{1}{B_0(1+p_f)^2}}{4\pi^2 \epsilon \int_{p_f}^{0} f(p'+1)dp'} \right]^{1/2}, \quad (48)$$

is independent on N and the modulation frequency ω, and p_f is evaluated at t_s according to Eq. (44).

To illustrate this result, let us consider the SSR case for which $f(p) = 1$. Here Eq. (47) becomes

$$\bar{r}_{\mathrm{ex}} = \left\{ \frac{(1-\epsilon)}{4\pi^2 \epsilon} [B_0(1-\epsilon)-1]^3 \right\}^{1/2} e^{-N[S_0+\Delta S]}, \quad (49)$$

where S_0 is given by Eq. (23) in accordance with Eq. (9) for the SSR case, and $\Delta S = -1/B_0 \ln(1-\epsilon) - \epsilon$. Note that for $\epsilon \ll 1$, this result reduces to $\Delta S = -\epsilon(1 - 1/B_0)$ in agreement with the LT result obtained in Sec. III A 1. In Fig. 6 we compare theoretical results in the adiabatic limit with Monte Carlo simulations for the case of a binomial SSD, and excellent agreement is observed.

The adiabatic theory is applicable as long as ω is much smaller, at all times, than the system's instantaneous relaxation

rate, $B_0[1 + \epsilon \cos(\omega t)] - 1$. This yields

$$B_0(1-\epsilon) - 1 \gg \omega, \quad (50)$$

which also entails that $B_0(1-\epsilon) > 1$. That is, ϵ cannot be too close to 1; otherwise, the adiabatic approximation breaks down. In addition, we must have $S[p_f(t_s),t_s] \gg N^{-1}$ for the eikonal approximation to be valid. Finally, for the saddle-point approximation to be valid, the width around the saddle, $|S_{tt}[p_f(t_s),t_s]|^{-1/2}$, has to be much smaller than π/ω, the distance between the saddle point and the integration boundaries in Eq. (40).

IV. CATASTROPHE

Having considered time-periodic reaction rates, we now turn to the case of a catastrophe, which we model by a temporary drop in the population's birth rate. Here the quantity of interest is not the MTE but rather the change in the extinction risk due to the catastrophe. Indeed, if the population dwells in a long-lived metastable state prior to extinction, before the catastrophe occurs the slowly time-dependent extinction probability satisfies $\mathcal{P}_0(t) \equiv 1 - e^{-t/\tau}$, where τ is the MTE of the population [18,34]. The catastrophe brings about an increase in the extinction risk $\Delta\mathcal{P}_0$ due to the temporary decrease in the birth rate, and it is our goal in this section to calculate this change. Here we generalize the treatment in Ref. [17] which included the SSR case and calculate the growth in the extinction risk for a general SSD.

In Fig. 7 we plot two typical stochastic trajectories of an established population undergoing a catastrophe, manifested by a sudden drop in the birth rate for a prescribed duration T. In Fig. 7(a) we show an example of a population that recovers from a catastrophe, while in Fig. 7(b) the latter brings about a rapid population extinction. Note that under the assumption that the extinction probability remains small in the aftermath of the catastrophe (see below), the effect of the latter on the MTE is negligible. This is because in this regime, the majority of trajectories recover after the catastrophe.
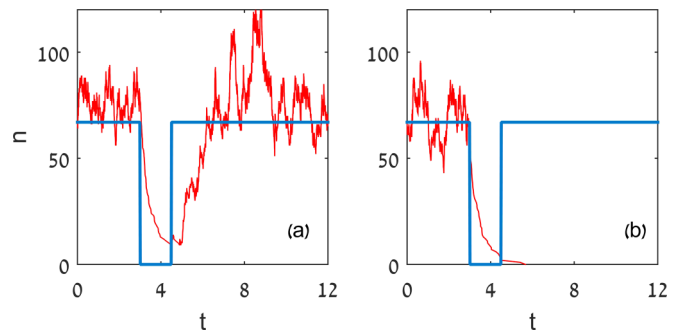

FIG. 7. Example of two trajectories (thin solid lines) showing the dynamics of the population in the aftermath of a catastrophe in the case of a binomial SSD. The catastrophe is manifested by a sudden drop, at some given time, in the birth rate (illustrated by the thick solid line) for a given duration T. While in (a) the population recovers, in (b) the catastrophe brings about population extinction. The parameters are $N = 100$, $B_0 = 3$, $T = 1.5$, $m = 10$, and $\rho = 0.2$.

To represent a catastrophe of duration T, we substitute

$$g(t) = \begin{cases} 1 & t < 0 \text{ or } t > T \\ 0 & 0 < t < T \end{cases} \qquad (51)$$

into Hamiltonian (5), and we set it to start at some arbitrary time $t_0 = 0$. To proceed we calculate the different segments of the Hamiltonian, before, after, and during the catastrophe and then demand continuity between the different instanton solutions. The Hamiltonian before and after the catastrophe is the time-independent Hamiltonian [Eq. (11)]. Whereas during the catastrophe the birth rate vanishes and the Hamiltonian becomes

$$H_c(p,q) = -pq[1 + B_0(p+1)q], \qquad (52)$$

which is independent on the specific choice of SSD. Now, in order to find the complete instanton, it is necessary to match the instaton during the catastrophe to the pre- and postcatastrophe instanton. The latter is the zero energy line of Eq. (11), given by Eq. (8). During the catastrophe, however, the *a priori* unknown energy, $E_c = H_c$, is no longer zero. It can be found by matching the nonzero energy line during the catastrophe

$$q_c = \frac{1}{2B_0(p+1)} \left[\sqrt{1 - \frac{4B_0(p+1)E_c}{p}} - 1 \right] \qquad (53)$$

with q_0 given by Eq. (8). Solving $q_0 = q_c$ gives us the intersections points $p_1(E_c)$ and $p_2(E_c)$

$$1 + \sqrt{1 - \frac{4B_0(p_{1,2}+1)E_c}{p_{1,2}}} = 2B_0(p_{1,2}+1)f(p_{1,2}+1), \qquad (54)$$

which can be explicitly found for any particular choice of SSD. In order to determine E_c we demand that the duration of the catastrophe be T. Putting $B(t) = 0$ in Hamilton equation (7) evaluated at $q = q_c$, using Eq. (53), and integrating from $t_0 = 0$ to $t = T$, we obtain

$$T = \int_{p_1(E_c)}^{p_2(E_c)} \frac{dp}{\sqrt{p^2 - 4pB_0(p+1)E_c}}, \qquad (55)$$

whose solution yields the energy E_c associated with the catastrophe. Having found E_c, the action is given by [17]

$$S(T) = S_0 - \int_{p_2(E_c)}^{p_1(E_c)} \{q_0(p) - q_c(p)\}dp - E_cT. \qquad (56)$$

According to the eikonal theory, this result for the decrease in action, together with Eq. (55), allows finding the increase in the extinction risk of the population up to exponential accuracy:

$$\Delta\mathcal{P}_0 \sim e^{-NS(T)}. \qquad (57)$$

Note that this result is valid as long as $NS(T) \gg 1$. Also note that if $\Delta\mathcal{P}_0 \gg \mathcal{P}_0$ (that is, if the catastrophe significantly increases the extinction risk), then Eq. (57) approximately describes the extinction risk in the aftermath of the catastrophe. In Fig. 8 we compare Eq. (57) with Monte Carlo simulations for the case of a binomial SSD. As expected, the theory holds as long as the duration T is not too long such that $NS(T) \gg 1$.

While we have given a general recipe to find the increase in the population's extinction risk for a generic SSD, it is
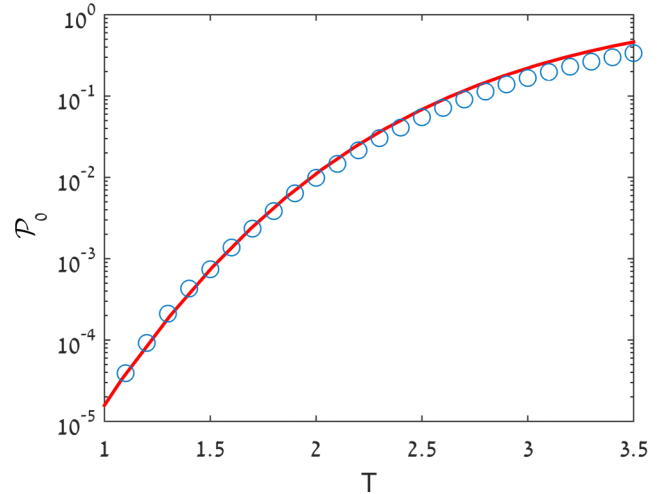

FIG. 8. Probability of extinction for the binomial SSD in the aftermath of a catastrophe: theory (solid line) and Monte Carlo simulations (symbols), as a function of the catastrophe duration T. The parameters are $B_0 = 1.1$, $N = 12\,000$, $m = 10$, and $\rho = 0.3$. The theoretical result is multiplied by a constant prefactor to match the simulation result at $T = 1.1$.

informative to examine these results close to the bifurcation limit where $B_0 - 1 \ll 1$. In Appendix B we show that in this limit the analytical solution drastically simplifies, and the action can be written as

$$S(T) = \frac{2S_0}{e^T + 1}, \qquad (58)$$

with S_0 given by Eq. (26). This result is a generalization of the result obtained by Assaf *et al.* [17] for the case of the SSR, corresponding to $f(p) = 1$.

V. NUMERICAL CALCULATIONS

To verify our analytical results we have used two different numerical methods. The first method is a time-dependent Monte Carlo simulation. It is based on an extended version of the time-independent Gillespie algorithm [49,50], which accounts for time-dependent reactions rates, see, e.g., Refs. [51,52]. In short, Gillespie's algorithm is composed of two steps: (i) advancing the time until the next reaction and (ii) choosing a reaction from all possible reactions and updating the population size accordingly. The second step is insensitive to whether the reaction rates are explicitly time dependent; here, accounting for bursty reproduction was done by considering all possible birth processes as independent reactions. To account for the time-dependent rates, we denote by $a_{\alpha\beta}$ the transition probability per unit time from state β to state α, and by $a_\alpha = \sum_\beta a_{\alpha\beta}$, the transition probability to reach α from all other states. At any given time t, the probability P_α that the system is still in configuration α after time δt has elapsed is thus [51,52]

$$P_\alpha(t) = \exp\left[-\int_t^{t+\delta t} dt' a_\alpha(t')\right]. \qquad (59)$$

In order to choose the time step δt in which the next reaction will occur, we generate a random number from a uniform

distribution in the interval [0,1] and demand that this random number be equal to P_α. In the time-independent case, δt can be explicitly found from this equation [49], but for time-dependent rates, this yields a transcendental equation [52], which has to be solved for each time step. Having found the time step δt, the next reaction is chosen according to the original Gillespie step, with the reactions rates evaluated at time $t + \delta t$ [51].

When the MTE is long, employing such an algorithm, which includes solving a transcendental equation at each time step, may be extremely time-consuming. As a result, we have also devised a numerical method to solve the explicitly time-dependent Hamilton equations numerically. For a time-independent Hamiltonian, finding the instanton numerically can be done directly using the shooting method. Here we start at time $t = 0$ in the close vicinity of the mean-field fixed point $(q_{mf} + \delta q, \delta p)$, where $\delta q, \delta p \ll 1$. To find the unstable eigendirection of the instanton, along which it leaves the vicinity of the mean-field fixed point at $t = 0$ and enters at some final time the close vicinity of the fluctuational point $(0, p_f)$, we substitute $q = q_{mf} + \delta q$ and $p = \delta p$ into the unperturbed instanton [Eq. (8)]. Retaining leading-order terms, we arrive at $\delta q = [f'(1) + 1/B_0]\delta p$, which determines the desired eigendirection. Having found the numerical solution to Eqs. (6) and (7) for some initial condition in the close vicinity of $(q_{mf}, 0)$ on the unperturbed instanton, one can find the action according to Eq. (9).

In the time-dependent case, however, the perturbed instanton is more intricate to find. Here we start from the same initial conditions as for the time-independent case, but we now pay attention to the relative phase between the unperturbed instanton and the perturbed trajectory. As a result, we solve Eqs. (6) and (7) for various relative phases and only then choose such a phase that minimizes the action of the perturbed instanton. This relative phase in the numerical solution is easily related to the minimization of the LT in Sec. III A, as both represent the deviation of the perturbed trajectory from the original time-independent trajectory (see Fig. 3). In Fig. 9 we give an example of a typical time-dependent trajectory in the (q, p, t) phase plane obtained in the manner described above. Additional examples for instantons in the high-frequency regime and with intermediate perturbation strength ($\epsilon = 0.5$) are shown in Fig. 5. Finally, we have checked that in the course of numerically finding the instantons, our algorithm gave a relative error on the order of 0.1% of the unperturbed action S_0. As a result, throughout this work we have only taken such results into account where $\Delta S/S_0 \gtrsim 10^{-2}$, which guarantees that the correction to the action includes an error of 10% at most.

VI. SUMMARY AND DISCUSSION

In this paper we have investigated the dynamics of a stochastic population under the joint influence of two nondemographic effects: a time-varying environment that gives rise to time-dependent reaction rates and bursty reproduction that gives rise to uncertainty in the reaction step size. Two time-modulation protocols have been considered: a periodically varying birth rate and a sudden temporary drop of the birth rate to zero. By using various analytical tools as well as extensive numerical
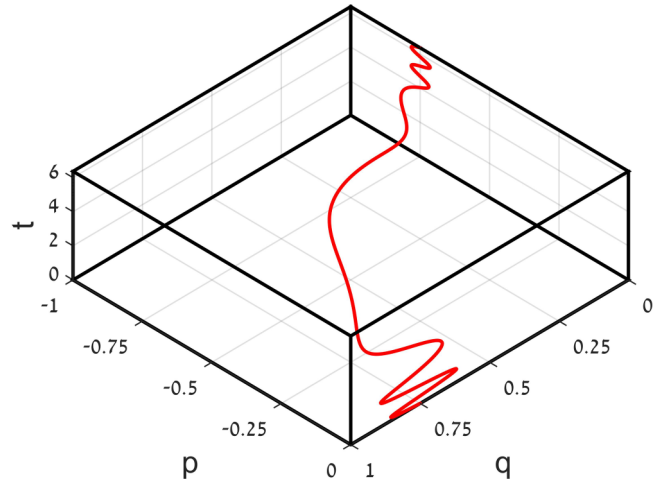

FIG. 9. An example of an instanton trajectory of the perturbed Hamiltonian in the SSR case. The parameters are $B_0 = 4$, $\epsilon = 0.3$, and $\omega = 6$. The trajectory first performs large-amplitude oscillations around the mean-field fixed point $(q, p) = (0.75, 0)$ and finally enters the vicinity of the fluctuational point $(q, p) = (0, -0.75)$.

simulations we have shown that such time modulation always decreases the MTE compared to the time-independent case. As a result, a time-varying environment always increases the extinction risk of a population. By accounting for bursty reproduction with an arbitrary SSD, this work generalizes previous works in this field which have treated constant-step-size reactions such as the Verhulst or the branching-annihilation models.

How does bursty reproduction affect the extinction risk in the presence of time-dependent rates? In the time-independent case it has been shown by Be'er and Assaf that bursty reproduction increases the extinction risk compared to the case of SSR (single-step birth reaction) [33]. However, when compared with a birth reaction that produces exactly K individuals (K-step reaction), depending on the skewness of the SSD, it has been shown that bursty reproduction can also decrease the extinction risk of the population [36]. Here we generalize these results by considering time-dependent rates and using a beta-binomial (BBN) distribution, which is a generalized version of the binomial distribution, see below.

In Fig. 10 we study the dependence of the extinction risk on the first two moments of the SSD. In Figs. 10(a) and 10(b) we show that the MTE is exponentially reduced as the mean of the SSD is increased by comparing the K-step reaction results with those using SSR. The reason for this increase in the population's extinction risk is that as the SSD's mean increases, birth events become less frequent and it is more likely to observe a series of death events that leads to population extinction. Yet, looking at the *ratio* of the MTEs, this effect is significantly reduced when the rates are time dependent, see Fig. 10(b).

In Figs. 10(c) and 10(d) we study how the width of the SSD affects the extinction risk by comparing the results of the K-step reaction with those using the BBN distribution. The latter is defined by three parameters: the number of independent trials m, and α, β which are the parameters of the beta distribution from which the probability of success of a single trial is taken. By tuning the parameters such
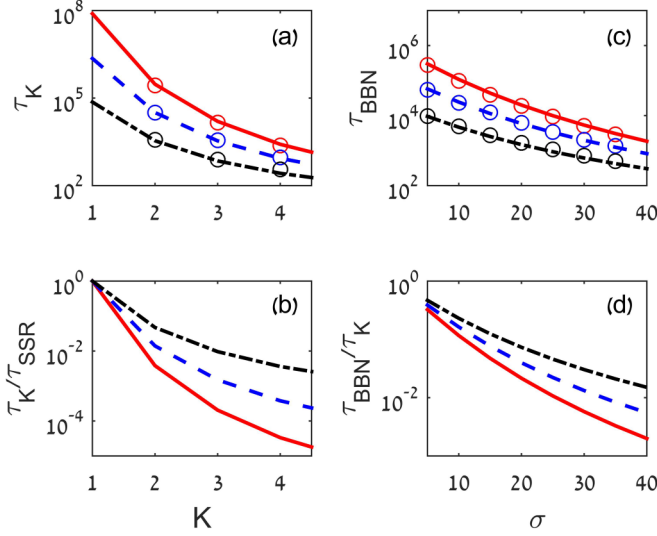
FIG. 10. Panel (a) shows the MTE for the case of a K-step reaction, see text, as a function of K. Here the different lines correspond to the theoretical results in the adiabatic limit for $\epsilon = 0.05, 0.15, 0.25$ (solid, dashed, and dash-dotted lines, respectively), while the symbols are results of Monte Carlo simulations. Panel (b) shows the MTE in (a) normalized by the MTE in the case of the SSR, namely $K = 1$. Parameters in (a) and (b) are $B_0 = 3$, $N = 70$, and $\omega = 0.01$. Panel (c) shows the MTE for the case of a BBN distribution, see text, as a function of the standard deviation σ, where the SSD's parameters (m, α, β) are chosen to maintain a constant mean of $K = 5$ (see text). The different lines correspond to the theoretical results in the adiabatic limit for $\epsilon = 0.05, 0.15, 0.25$ (solid, dashed, and dash-dotted lines, respectively), while the symbols are results of Monte Carlo simulations. Panel (d) shows the MTE in (c) normalized by the MTE in the case of a K-step reaction with $K = 5$ and $\sigma = 0$. Parameters in (c) and (d) are $B_0 = 6$, $N = 80$, and $\omega = 0.01$.

that the mean of the BBN coincides with K, we show that the MTE is exponentially decreased when the SSD's width is increased, see Fig. 10(c). The reason for this increase in the population's extinction risk is that as the SSD's width increases, large-burst-size birth events become more likely and thus, it is more likely to observe a series of death events that drives the population to extinction. Yet, looking at the *ratio* of the MTEs, again the effect of MTE reduction is drastically reduced when introducing time-dependent rates, see Fig. 10(d).

We have also examined how the SSD's third moment affects the population's extinction risk. In Fig. 11 we compare the BBN results with those of a symmetric three-value triangular (TR) SSD. To study the net effect of the third moment, the TR distribution is tuned such that the mean and variance coincide with that of the BBN distribution. Figure 11 demonstrates that when the SSD is positively skewed, the MTE is increased and vice versa, while for zero skewness the MTEs almost coincide. This is because for positively skewed SSDs (here the BBN), the median is smaller than the mean, and thus small-burst-size birth events are more likely than in the TR case, where the median is equal to the mean. Yet, similarly to the cases of the first and second moments, as the time modulation amplitude ϵ increases, the effect of increasing the MTE as the skewness increases is diminished [53].
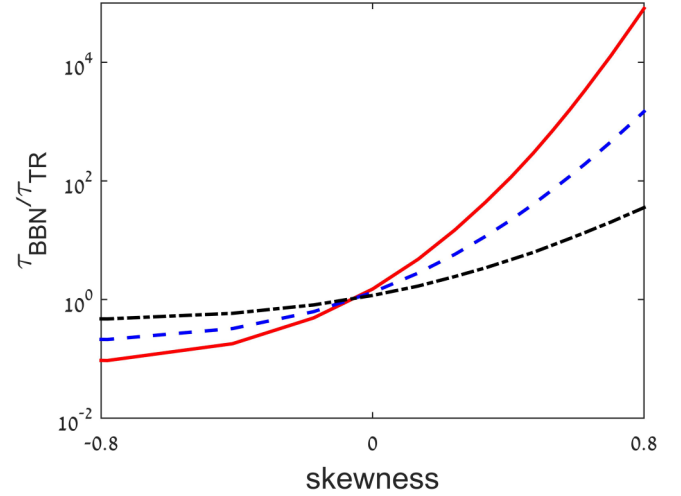

FIG. 11. The ratio between the MTEs in the cases of a BBN and a three-value TR (see text) distribution, as function of the BBN's skewness. The lines correspond to theoretical results in the adiabatic limit for $\epsilon = 0.05, 0.25, 0.45$ (respectively, solid, dashed, and dash-dotted lines). The parameters are $B_0 = 6$, $N = 1000$, $\omega = 0.01$, and the SSD parameters are chosen such that the SSD's mean and variance be equal at each point.

To understand the interplay between having time-dependent rates and bursty reproduction, we consider the adiabatic limit (Sec. III C). Here the system "waits" until the effective birth rate goes to its minimum, $B_0(1 - \epsilon)$ (see Sec. III C), and only then it goes to extinction. Thus, the typical population size, which directly depends on the birth rate, and from which the system goes extinct, is decreased. Therefore, since the MTE is exponentially sensitive to the typical population size, we find that the effect of increase or decrease in the extinction risk is exponentially diminished due to the time-dependent rates. Finally, note that while Figs. 10 and 11 demonstrate the adiabatic regime, we have checked that this effect (although weaker) still exists in the nonadiabatic regime as well.

APPENDIX A: KAPITSA RESULTS

In this Appendix we provide some intermediate results for the high-frequency limit, $\alpha = \omega/(B_0 - 1) \gg 1$. Using Eqs. (27) and (31), we perform an almost canonical transformation from the old variables q and p to the new variables Q and P:

$$p(Q, P, t) = P\left[1 - \frac{\epsilon}{\alpha}(P + 1)f \sin(\omega t)\right], \quad \text{(A1)}$$

$$q(Q, P, t) = \frac{Q}{1 - \frac{\epsilon}{\alpha}\sin(\omega t)[(2P + 1)f + P(P + 1)f']}$$

$$\simeq Q\left\{1 + \frac{\epsilon}{\alpha}\sin(\omega t)[(2P + 1)f + P(P + 1)f']\right.$$

$$\left. + \left(\frac{\epsilon}{\alpha}\right)^2 \sin^2(\omega t)[(2P + 1)f + P(P + 1)f']^2\right\}.$$

$$\text{(A2)}$$

This transformation is canonical up to third order in $\mathcal{O}[(1/\alpha)^3] \ll 1$, since the Poisson brackets satisfy $\{q, p\}_{Q,P} =$

$1 + \mathcal{O}[(1/\alpha)^3]$. The generating function of this transformation satisfies [43]

$$F_2(q, P, t) = q P \left[1 - \frac{\epsilon}{\alpha}(P + 1) f \sin(\omega t) \right]. \tag{A3}$$

This allows making the transformation $H' = H + \partial F_2/\partial t$, where by time averaging the new Hamiltonian H' over a period of rapid oscillation $2\pi/\omega$, we arrive at the effective time-independent Hamiltonian [Eq. (32) in the main text]. Here the correction to the unperturbed Hamiltonian, due to the high-frequency time modulation, reads:

$$
\begin{aligned}
H_2 = &\tfrac{1}{2} Q P \big[B_0 P(1 + P)^2 f^3 - P(1 + P) \\
&\times [1 + 3P + 4B_0 Q(1 + P)(1 + 2P)] f f' \\
&- P^2(1 + P)^2[1 + 3B_0 Q(1 + P)](f')^2 \\
&+ f^2\big(-\{P + 2P^2 + B_0 Q(1 + P)[1 + 5P(1 + P)]\} \\
&+ B_0 P(1 + P)^2\big[(1 + 2P)f' + \tfrac{1}{2}P(1 + P)f''\big]\big) \big].
\end{aligned}
\tag{A4}
$$

Finally, this correction brings about a correction to the unperturbed instanton (8), which has the form

$$
\begin{aligned}
&Q_K(P) \\
&= \frac{1}{4B_0}(-2B_0(1 + 2P)^2 f^3 + 4P^2(1 + P)(f')^2 \\
&+ 2P f f'[3 + 5P - 3B_0 P(1 + P)^2 f'] + f^2\{2 + 6P \\
&+ B_0 P(1 + P)[-6(1 + 2P)f' + P(1 + P)f'']\}).
\end{aligned}
\tag{A5}
$$

This result allows us to explicitly calculate the correction to the action in Eq. (34), see Sec. III B in the main text.

APPENDIX B: CATASTROPHE CALCULATIONS IN THE BIFURCATION LIMIT

In this Appendix we calculate the action in the case of a catastrophe close to the bifurcation limit. Here the treatment goes along the same lines as in Sec. III A 2. We denote $p_0 = (B_0 - 1)/[1 + f'(1)]\tilde{p}_0$ and $q_0 = (B_0 - 1)\tilde{q}_0$, where $\tilde{p}_0$ and $\tilde{q}_0$ are $\mathcal{O}(1)$. We also denote $H = \tilde{H}(B_0 - 1)^2/[f'(1) + 1]$. Thus, in the leading order the Hamiltonian before and after the catastrophe reduces to

$$\tilde{H} = \tilde{p}\tilde{q}(\tilde{p} - \tilde{q} + 1)(B_0 - 1), \tag{B1}$$

while the normalized instanton is $\tilde{q} = 1 + \tilde{p}$. The Hamiltonian during the catastrophe [Eq. (52)] reduces in leading order to

$$\tilde{H}_c = -\tilde{p}\tilde{q}. \tag{B2}$$

Demanding that $\tilde{E}_c = \tilde{H}_c$, the nonzero energy trajectory during the catastrophe becomes $\tilde{q}_c = -\tilde{E}_c/\tilde{p}$. The intersection points between the instantons before or after and during the catastrophe are found by solving $\tilde{q}_c = \tilde{q}$:

$$\tilde{p}_{1,2} = -\tfrac{1}{2}(1 \pm \sqrt{1 - 4\tilde{E}_c}). \tag{B3}$$

During the catastrophe the Hamilton equation for the momentum reduces to $\dot{\tilde{p}} = \tilde{p}$, which yields $\tilde{p}_2/\tilde{p}_1 = e^T$. As a result we find [17]

$$\tilde{E}_c = \frac{e^T}{(1 + e^T)^2} = \frac{1}{4}\cosh^{-2}(T/2), \tag{B4}$$

$$\tilde{p}_1 = -\frac{1}{2}[1 + \tanh(T/2)], \quad \tilde{p}_2 = -\frac{1}{2}[1 - \tanh(T/2)]. \tag{B5}$$

Finally, using Eq. (56) we arrive at

$$S(T) = \frac{(B_0 - 1)^2}{2[1 + f'(1)]}[1 - \tanh(T/2)] = \frac{2S_0}{e^T + 1}, \tag{B6}$$

where we have used the definition of S_0 from Eq. (26).

[1] M. S. Bartlett, *An Introduction to Stochastic Processes: With Special Reference to Methods and Applications* (Cambridge University Press, Cambridge, 1978).

[2] W. Horsthemke and R. Lefever, *Noise-Induced Transitions: Theory and Application in Physics, Chemistry, and Biology* (Springer, Berlin, 1984), Vol. 15.

[3] C. W. Gardiner *et al.*, *Handbook of Stochastic Methods* (Springer, Berlin, 1985), Vol. 3.

[4] N. G. Van Kampen, *Stochastic Processes in Physics and Chemistry* (Elsevier, Amsterdam, 1992), Vol. 1.

[5] E. Parzen, *Stochastic Processes* (SIAM, Philadelphia, PA, 1999).

[6] M. Assaf and B. Meerson, Phys. Rev. Lett. **100**, 058105 (2008).

[7] I. B. Schwartz, L. Billings, M. Dykman, and A. Landsman, J. Stat. Mech.: Theory Exp. (2009) P01005.

[8] J. E. Pearson, P. Krapivsky, and A. S. Perelson, PLoS Comput. Biol. **7**, e1001058 (2011).

[9] M. Dykman, E. Mori, J. Ross, and P. Hunt, J. Chem. Phys. **100**, 5735 (1994).

[10] R. M. Nisbet and W. Gurney, *Modelling Fluctuating Populations: Reprint of First Edition (1982)* (Blackburn Press, 2003).

[11] V. Elgart and A. Kamenev, Phys. Rev. E **70**, 041106 (2004).

[12] C. R. Doering, K. V. Sargsyan, and L. M. Sander, Multiscale Model. Simul. **3**, 283 (2005).

[13] M. Assaf and B. Meerson, Phys. Rev. Lett. **97**, 200602 (2006).

[14] M. Assaf and B. Meerson, Phys. Rev. E **75**, 031122 (2007).

[15] D. A. Kessler and N. M. Shnerb, J. Stat. Phys. **127**, 861 (2007).

[16] M. Assaf, A. Kamenev, and B. Meerson, Phys. Rev. E **78**, 041123 (2008).

[17] M. Assaf, A. Kamenev, and B. Meerson, Phys. Rev. E **79**, 011127 (2009).

[18] M. Assaf and B. Meerson, Phys. Rev. E **81**, 021116 (2010).

[19] M. Assaf, B. Meerson, and P. V. Sasorov, J. Stat. Mech.: Theory Exp. (2010) P07018.

[20] B. Meerson and O. Ovaskainen, Phys. Rev. E **88**, 012124 (2013).

[21] S. Be'er, M. Assaf, and B. Meerson, Phys. Rev. E **91**, 062126 (2015).

[22] P. Hänggi and P. Jung, Adv. Chem. Phys. **89**, 239 (1995).

[23] M. B. Elowitz, A. J. Levine, E. D. Siggia, and P. S. Swain, Science **297**, 1183 (2002).

[24] E. G. Leigh, J. Theor. Biol. **90**, 213 (1981).

[25] R. Lande, Science **241**, 1455 (1988).

[26] R. Lande, Am. Nat. **142**, 911 (1993).

[27] R. Lande, S. Engen, and B.-E. Sæther, Oikos **83**, 383 (1998).

[28] A. Kamenev, B. Meerson, and B. Shklovskii, Phys. Rev. Lett. **101**, 268103 (2008).

[29] M. Assaf, E. Roberts, Z. Luthey-Schulten, and N. Goldenfeld, Phys. Rev. Lett. **111**, 058102 (2013).

[30] E. Y. Levine and B. Meerson, Phys. Rev. E **87**, 032127 (2013).

[31] N. Bacaër, J. Math. Biol. **71**, 491 (2015).

[32] S. Be'er, M. Heller-Algazi, and M. Assaf, Phys. Rev. E **93**, 052117 (2016).

[33] S. Be'er and M. Assaf, J. Stat. Mech.: Theory Exp. (2016) 113501.

[34] M. Assaf and B. Meerson, J. Phys. A: Math. Theor. **50**, 263001 (2017).

[35] L. Billings and E. Forgoston, Ric. Mat., 1 (2017).

[36] S. Be'er and M. Assaf, Phys. Rev. E **97**, 020302(R) (2018).

[37] J. Martin, B. Moorter, E. Revilla, P. Blanchard, S. Dray, P.-Y. Quenette, D. Allaine, and J. E. Swenson, J. Anim. Ecol. **82**, 290 (2013).

[38] M. González-Suárez and E. Revilla, Ecol. Lett. **16**, 242 (2013).

[39] E. J. Crespi, T. D. Williams, T. S. Jessop, and B. Delehanty, Funct. Ecol. **27**, 93 (2013).

[40] N. S. Goel and N. Richter-Dyn, *Stochastic Models in Biology* (Elsevier, Amsterdam, 2016).

[41] J. Paulsson and M. Ehrenberg, Phys. Rev. Lett. **84**, 5447 (2000).

[42] V. Shahrezaei and P. S. Swain, Proc. Natl. Acad. Sci. USA **105**, 17256 (2008).

[43] L. D. Landau and E. M. Lifshitz, *Mechanics*, Vol. 1 (3rd ed.) (Elsevier Butterworth-Heinemann, Oxford, 1976).

[44] Here, we use a shifted momentum in order to simplify the notation of the function $f(p)$, and also the Hamiltonian, see below.

[45] M. I. Dykman, H. Rabitz, V. N. Smelyanskiy, and B. E. Vugmeister, Phys. Rev. Lett. **79**, 1178 (1997).

[46] M. Dykman, B. Golding, L. McCann, V. Smelyanskiy, D. Luchinsky, R. Mannella, and P. McClintock, Chaos **11**, 587 (2001).

[47] C. Escudero and J. Á. Rodríguez, Phys. Rev. E **77**, 011130 (2008).

[48] In the time-independent case, $q_0(t - t_0)$ and $p_0(t - t_0)$ can be found by solving Hamilton equations $\dot{q}_0 = \partial_p H_0$, and $\dot{p}_0 = -\partial_q H_0$. Here t_0 serves as an arbitrary time shift.

[49] D. T. Gillespie, J. Phys. Chem. **81**, 2340 (1977).

[50] D. T. Gillespie, J. Comput. Phys. **22**, 403 (1976).

[51] A. Jansen, Comput. Phys. Commun. **86**, 1 (1995).

[52] D. F. Anderson, J. Chem. Phys. **127**, 214107 (2007).

[53] Close to the bifurcation limit, this effect vanishes since the MTE depends only on the first two moments of the SSD.